nature geoscience

Supplementary information

https://doi.org/10.1038/s41561-025-01781-6

Seismic evidence for oceanic plate delamination offshore Southwest Iberia

In the format provided by the authors and unedited

Supplementary Table 1: Physical parameters used in the numerical models.

Quantity	Symbol	Unit	Value
Gravity	g	$m.s^{-2}$	9.81
Thermal expansivity coefficient	α	K^{-1}	3.00×10^{-5}
Thermal diffusivity	κ	$m^2.s^{-1}$	1.00×10^{-6}
Sediments density at 273K	ρ_{uc}	$kg.m^{-3}$	2500
Dry mantle density at 273K	ρ_{dm}	$kg.m^{-3}$	3300
Hydrated mantle density at 273K	ρ_{hm}	$kg.m^{-3}$	2900
Top temperature	T_t	K	273
Bottom temperature	T_b	K	1748
Minimum viscosity	η_{min}	Pa.s	1.00×10^{19}
Maximum viscosity	η_{max}	Pa.s	1.00×10^{24}
Gas constant	R	$J.K^{-1}.mol^{-1}$	8.3145

Rheological parameters

Sediments (wet quartzite)			
Stress exponent	n		2.3
Pre-exponential factor	A	$MPa^{-n}.s^{-1}$	3.1623×10^{-7}
Activation energy	E	$kJ.mol^{-1}$	1.54×10^5
Activation volume	V	$m^3.mol^{-1}$	8.0×10^{-6}

Upper mantle (dry peridotite)			
Stress exponent	n		3.5
Pre-exponential factor	A	$MPa^{-n}.s^{-1}$	2.5×10^4
Activation energy	E	$kJ.mol^{-1}$	5.32×10^5
Activation volume	V	$m^3.mol^{-1}$	12.0×10^{-6}
Oceanic basaltic crust (plagioclase)			
Stress exponent	n		3.2
Pre-exponential factor	A	$MPa^{-n}.s^{-1}$	3.1623×10^{-6}
Activation energy	E	$kJ.mol^{-1}$	2.38×10^5
Activation volume	V	$m^3.mol^{-1}$	0
Hydrated/serpentinized mantle and weak zones (isoviscous)			
Viscosity	η	Pa.s	1.0×10^{19}

Plastic parameters

Cohesion	C	MPa	30.0
Cohesion after softening	C_s	MPa	0.1
Internal friction angle	α	°	25.0
Internal friction angle after softening	α_s	°	0.1

Max plastic strength (Peierls)

Cohesion	C	MPa	300.0

Supplementary Table 2: Additional numerical models testing different combinations of parameters.

<table>
<tr><td colspan="2"></td><th colspan="3">Number of Vertical Weak Zones</th></tr>
<tr><td colspan="2"></td><th>0</th><th>1</th><th>2</th></tr>
<tr><th rowspan="3">Thickness of the serpentinized layer</th><th>0 km</th><td>Model D1
(Extended Data Fig. 1)</td><td>Model D4
(Extended Data Fig. 4)</td><td>Model D7
(Extended Data Fig. 7)</td></tr>
<tr><th>5 km</th><td>Model D2
(Extended Data Fig. 2)</td><td>Model D5
(Extended Data Fig. 5)</td><td>Models D8
(Extended Data Fig. 8)</td></tr>
<tr><th>10 km</th><td>Model D3
(Extended Data Fig. 3)</td><td>Model D6
(Extended Data Fig. 6)</td><td>Models D9 + D10*
(Extended Data Figs. 9 and 10)</td></tr>
</table>

* Model D10 has the same geometry and parameters as model D9 but the convergence was stopped after 18 Myrs.

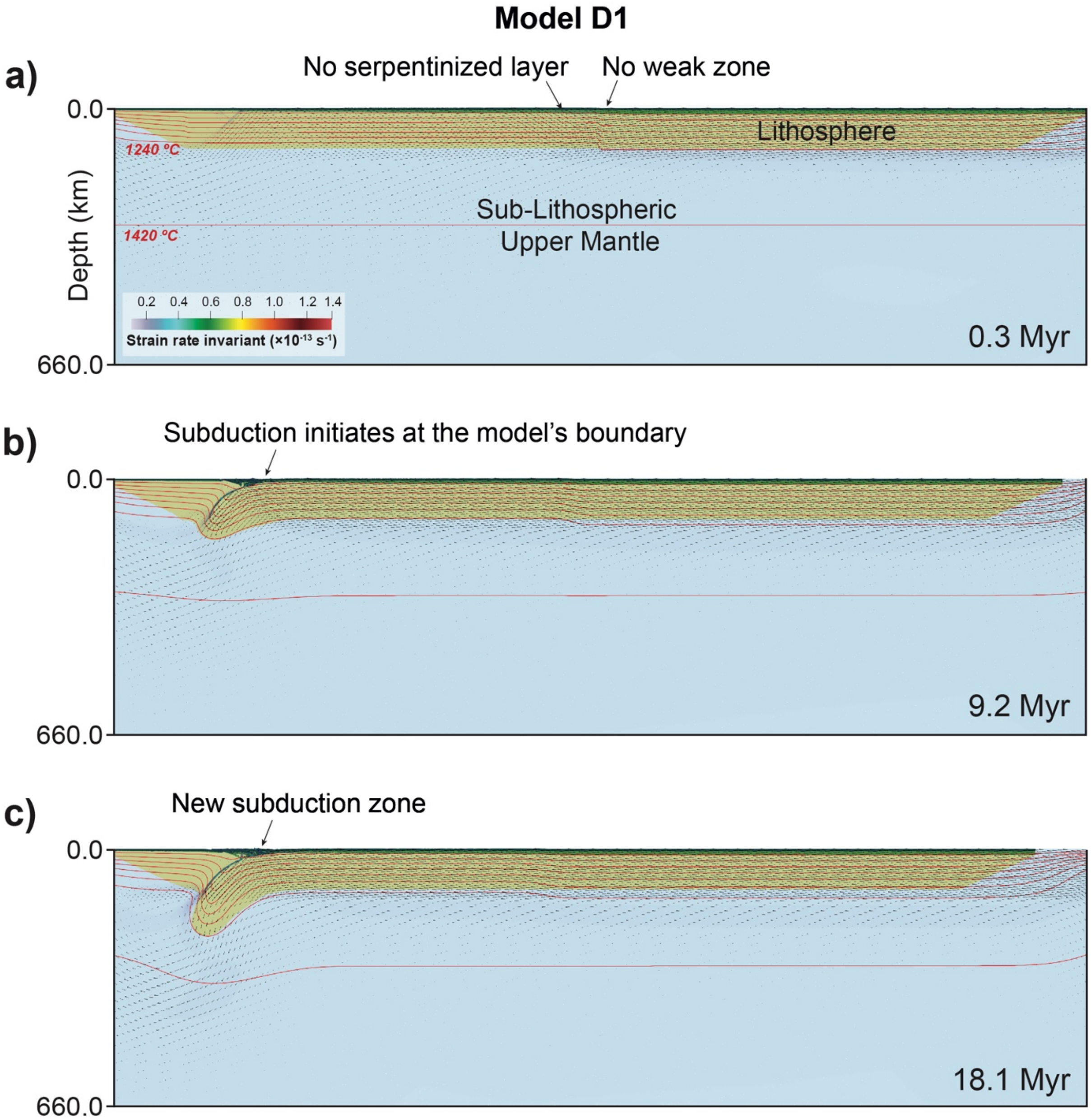

Supplementary Figure 1. Model D1 without weak zones and without a serpentinized layer. Note that there is no deformation localizing at the center of the model. Even though the lithosphere has different thicknesses, there is effectively no plate boundary. The convergence imposed on the African plate propagates into the Eurasian plate and deformation localizes near the boundary of the model due to boundary conditions.

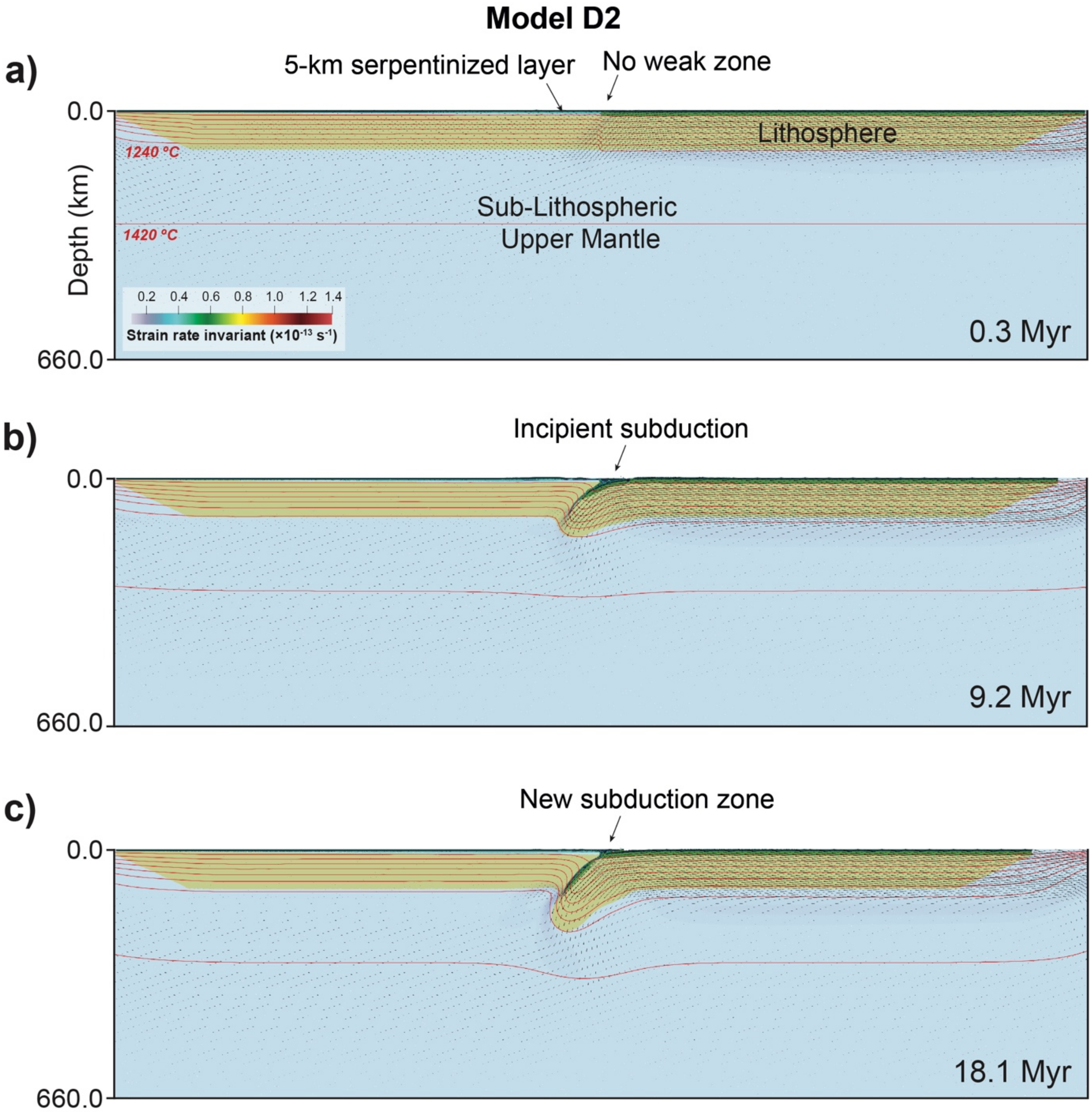

Supplementary Figure 2. Model D2 without weak zones and with a 5-km serpentinized layer. The deformation localizes in the center of the model at the contact between the two plates, even though there is no plate boundary there. This is probably because the 5-km serpentinized layer in the Eurasian plate acts as a weak zone. This leads to subduction initiation of Africa below Eurasia with the development of a plate interface and a small slab.

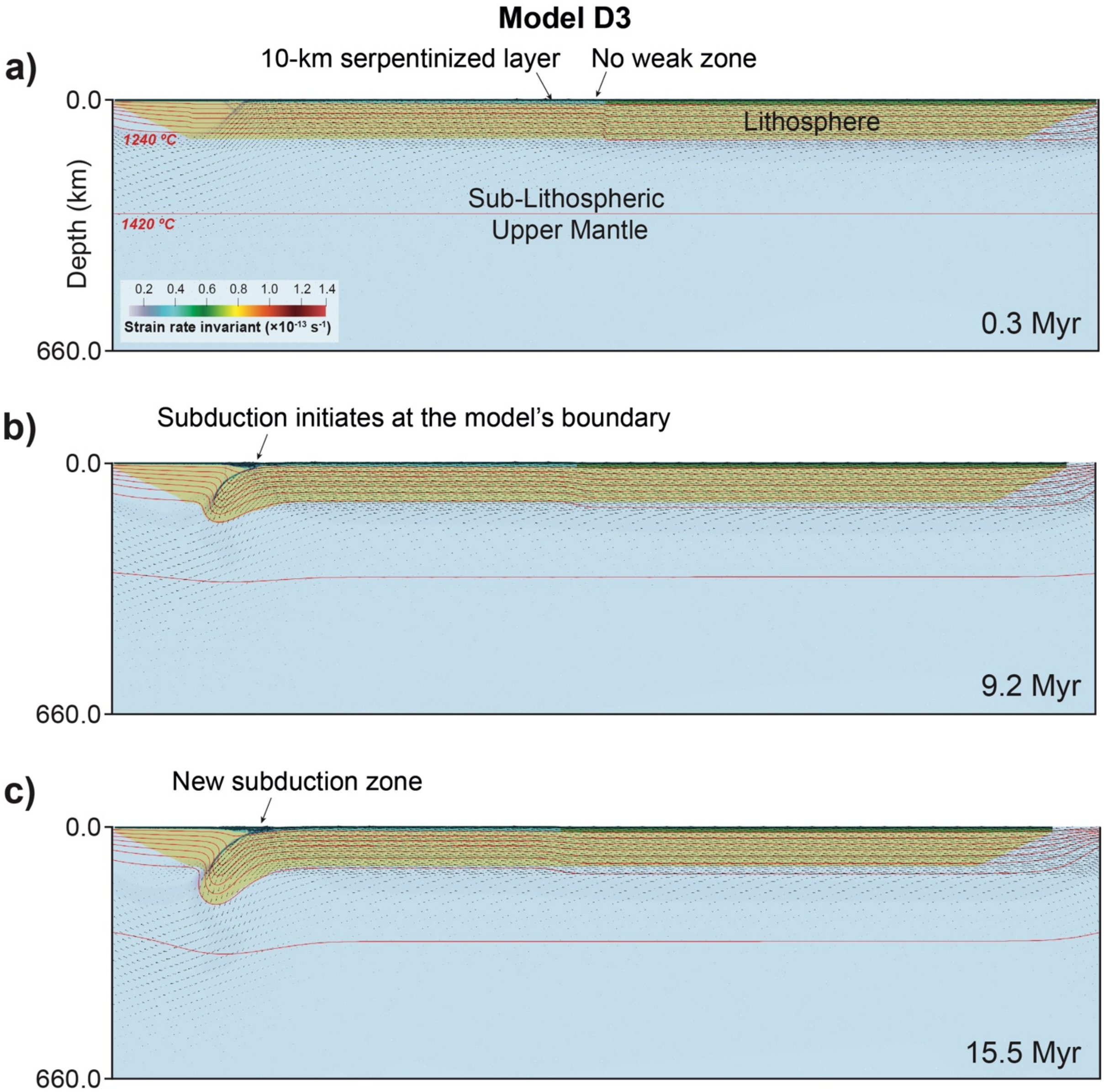

Supplementary Figure 3. Model D3 without weak zones and with a 10-km serpentinized layer. Deformation localizes near the boundary of the model. This is somehow unexpected, as one would think that a thicker serpentinized layer would facilitate subduction initiation. This has two possible explanations: 1) the facility of subduction initiation scales with the thickness of the serpentinized layer, or 2) the models without a proper plate boundary are unstable as the energy levels required to localize deformation in the center of the model and at the model's boundary (for this specific configuration) are of similar magnitude.

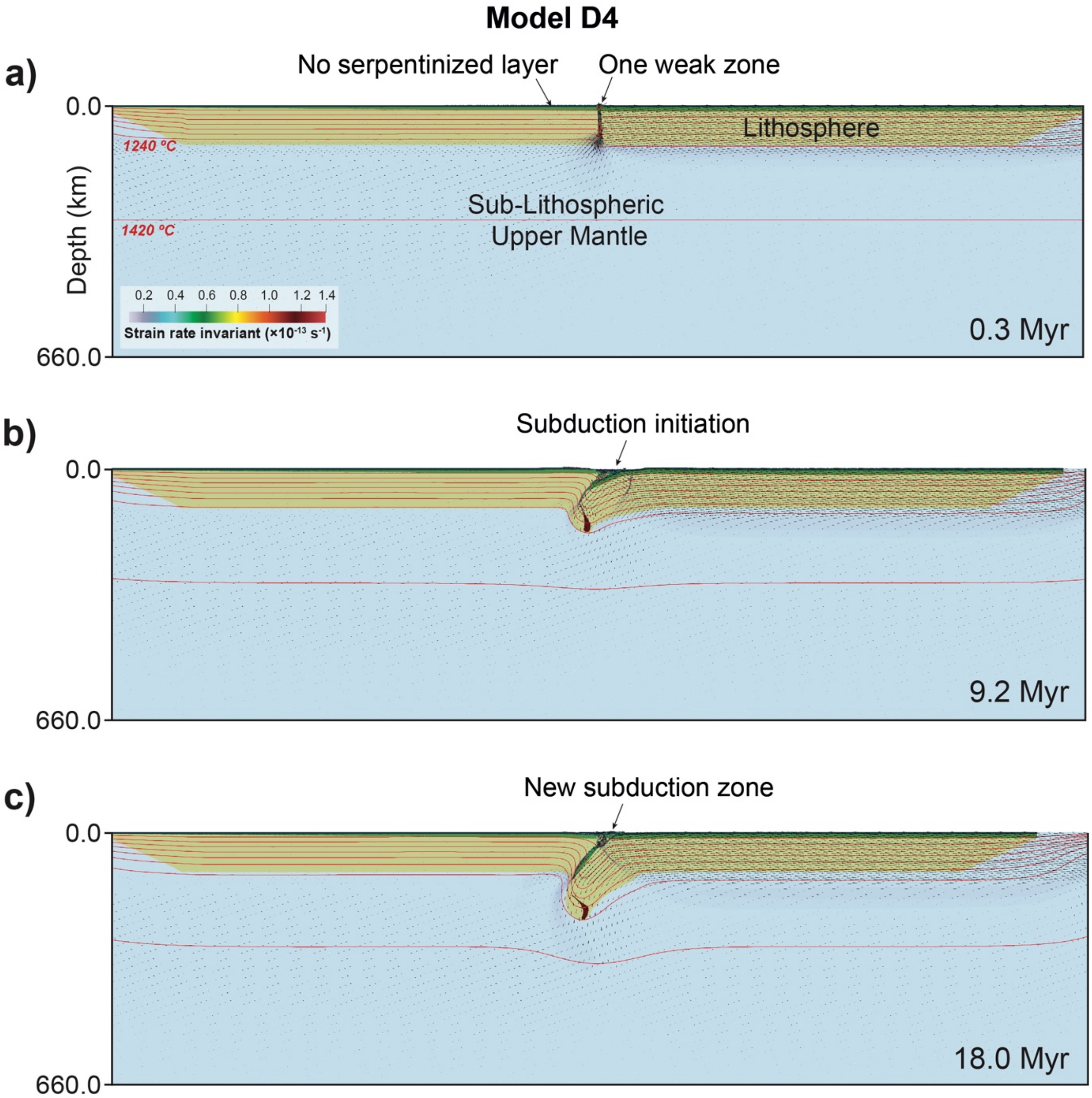

Supplementary Figure 4. Model D4 with a weak zone and no serpentinized layer. The presence of a vertical weak zone representing a discrete plate boundary leads to the subduction initiation of Africa below Eurasia.

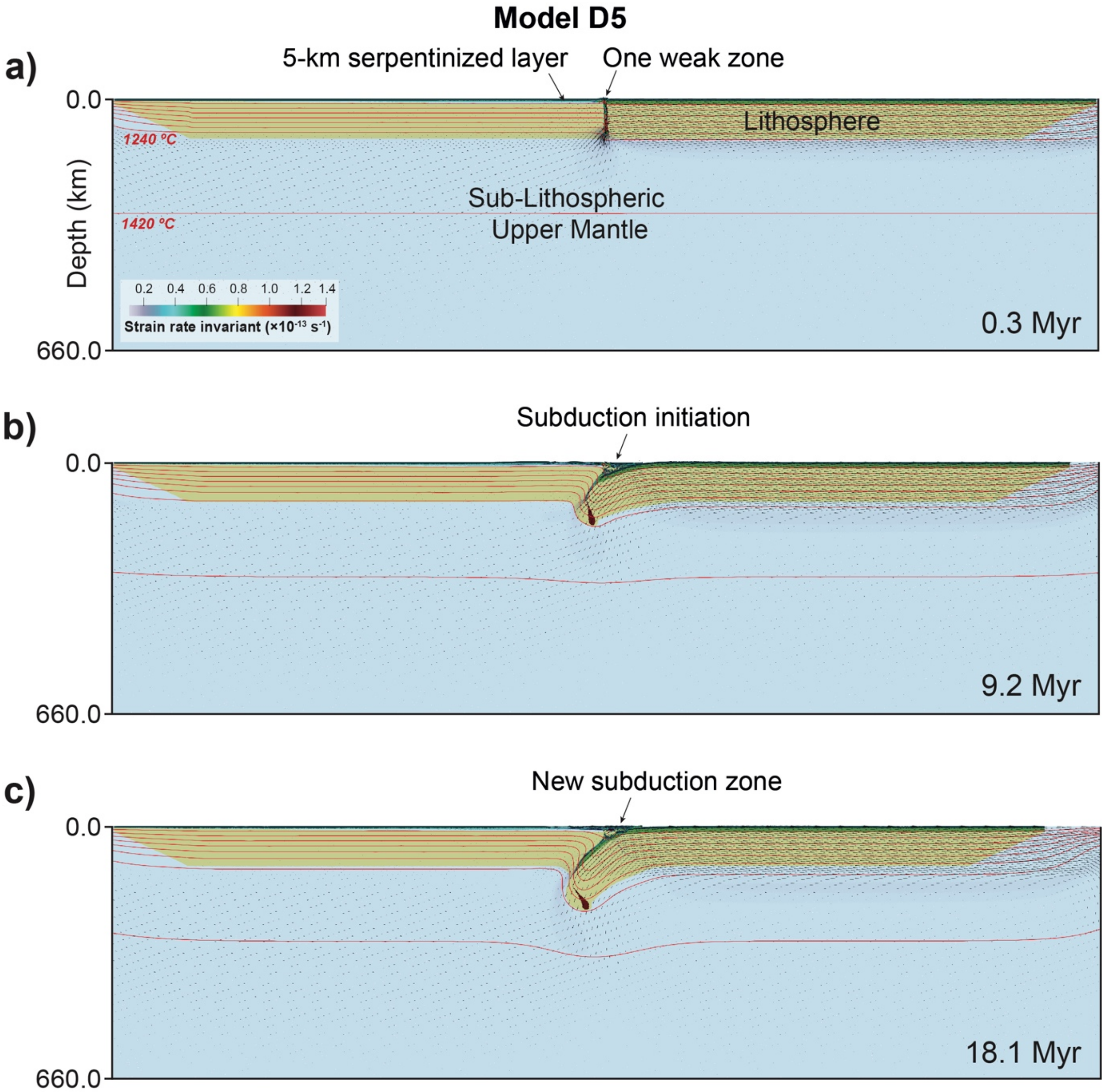

Supplementary Figure 5. Model D5 with a weak zone and a 5-km serpentinized layer. The presence of a vertical weak zone representing a discrete plate boundary leads to the subduction initiation of Africa below Eurasia. This model is similar to the previous one, suggesting that for this configuration a 5-km-thick serpentinized layer has little impact on the process.

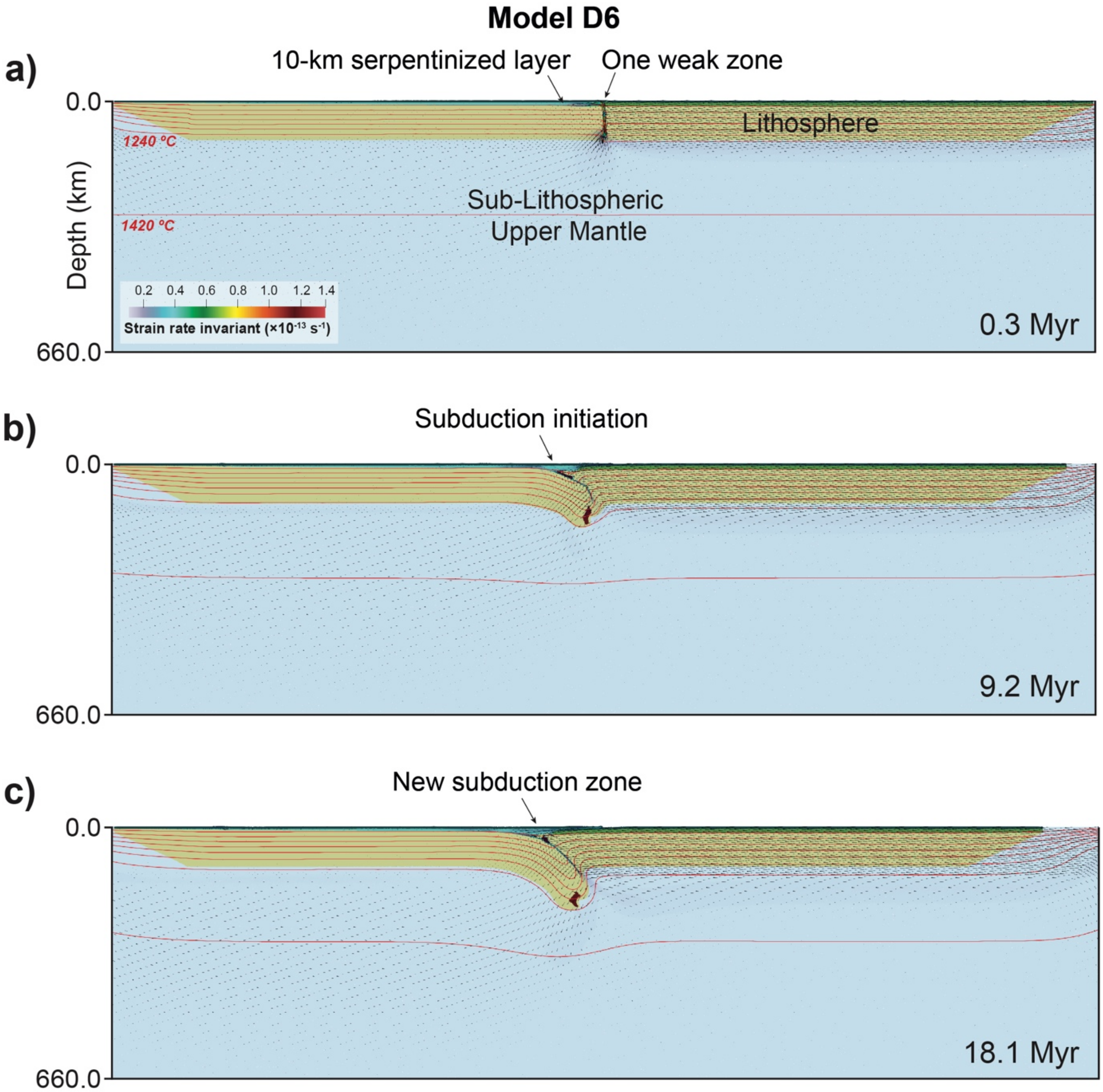

Supplementary Figure 6. Model D6 with a weak zone and a 10-km serpentinized layer. In this case, there is also the formation of a subduction zone at the plate's interface, but with the younger Eurasian plate subducting below Africa. This is likely an effect of the 10-km-thick serpentinized layer that decouples the crust from the lithospheric mantle, facilitating the bending of the thinner plate. This is a form of forced delamination and suggests that it is facilitated by a 10-km-thick serpentinized layer.

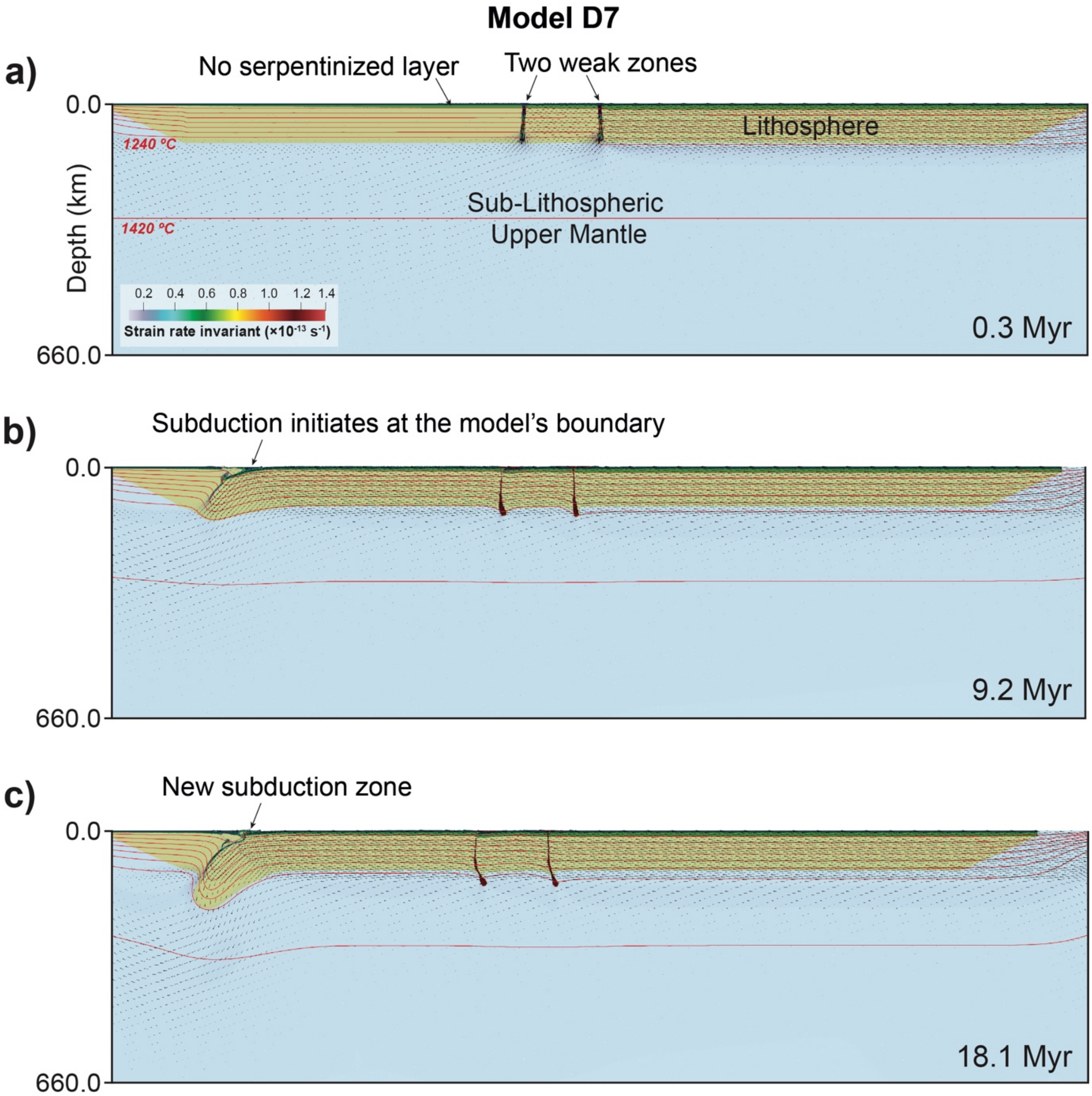

Supplementary Figure 7. Model D7 with two weak zones and no serpentinized layer. Deformation localizes at the boundary of the model, even though there are two weak zones at the center of the model. It is possible to observe that they get locked. No delamination is observed.

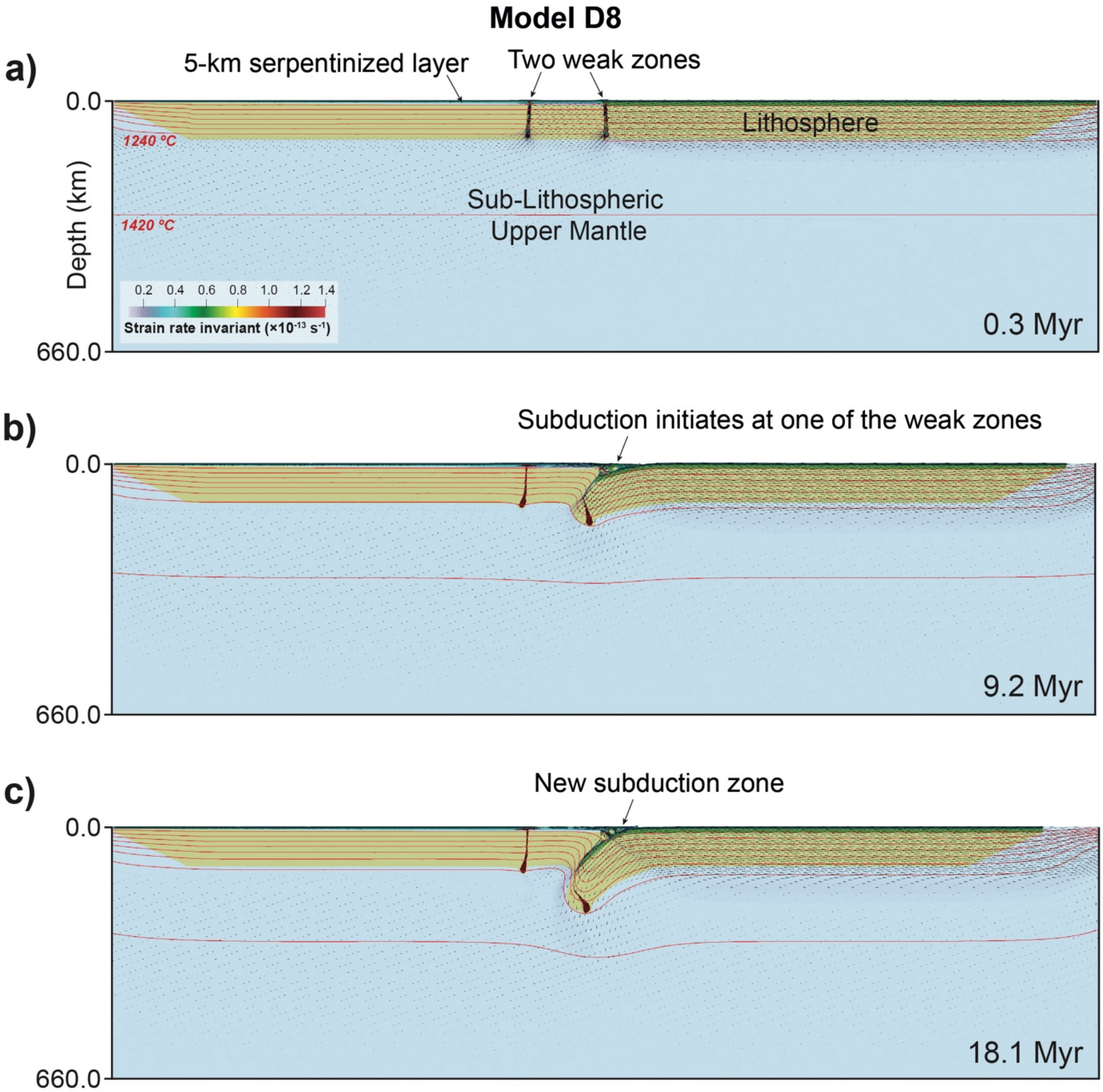

Supplementary Figure 8. Model D8 with two weak zones and a 5-km serpentinized layer. Deformation localizes and subduction initiates at one of the weak zones, with no significant delamination.

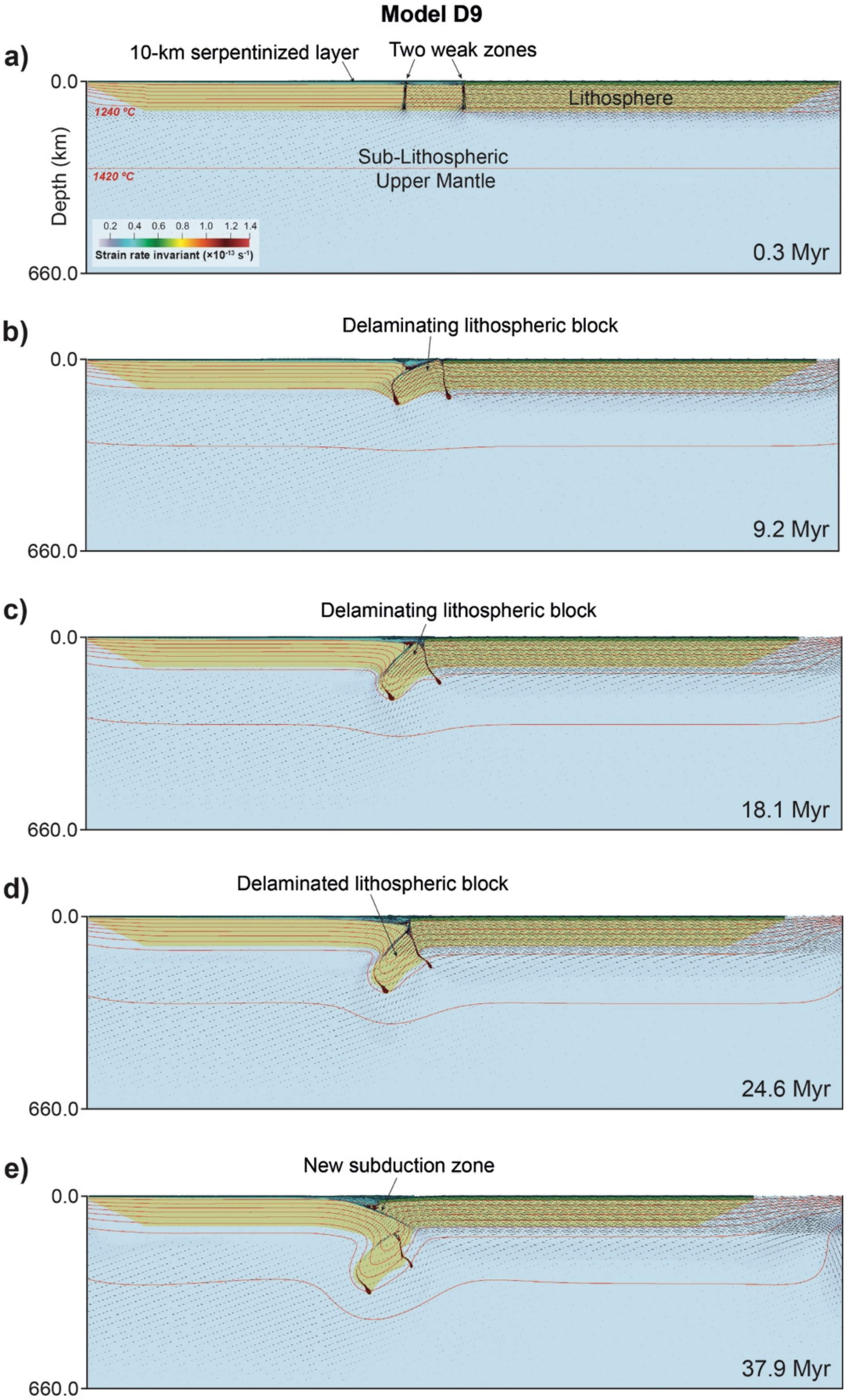

Supplementary Figure 9. Model D9 with two weak zones and a 10-km serpentinized layer (reference model shown in Fig. 3). The block between the two weak zones delaminates, after which subduction of Eurasia below Africa initiates. The process is facilitated by the 10-km-thick serpentinized layer.

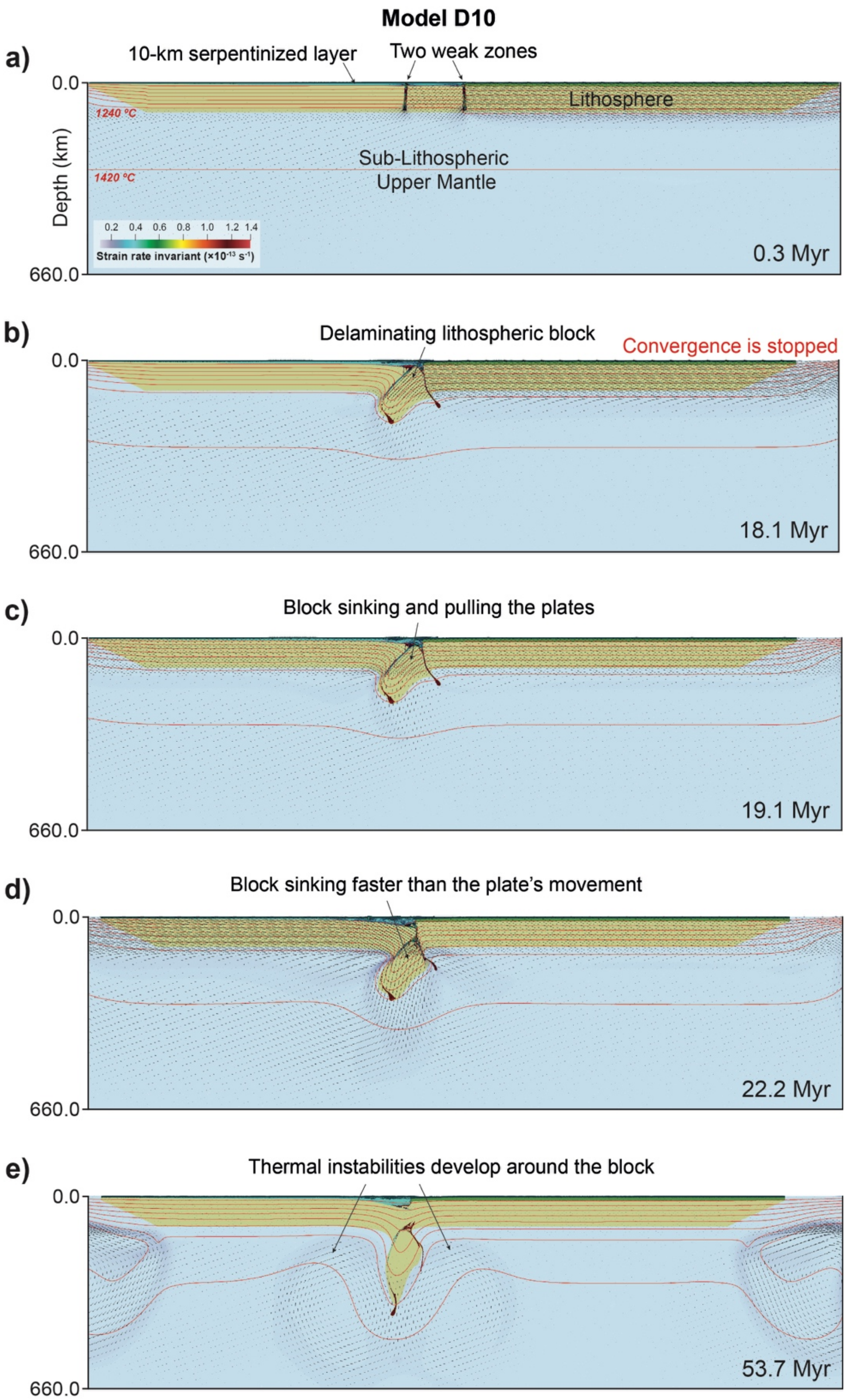

Supplementary Figure 10. Model D10 with two weak zones and a 10-km serpentinized layer with convergence stopped after 18 Myr. The delaminating lithospheric block continues to sink even after convergence is stopped due to its own negative buoyancy.

Supplementary Note: Estimated rupture area and implied seismogenic potential

We calculated the seismogenic potential of the north dipping blind-thrust potentially hidden below the Horseshoe Abyssal Plain that was inferred based on the computation of the 1969 focal mechanisms and on the distribution of its aftershocks[1,2]. The existence of this blind-thrust is consistent with our numerical models and with the distribution of the hypocenters of the NEAREST OBS experiment (see Fig. 2b). The dip of this fault was obtained from the 1969 focal mechanism and considered to be 52ºNE[1], while its length was approximated to the main length of the anomaly observed in the tomography (see Supplementary Fig. 4).

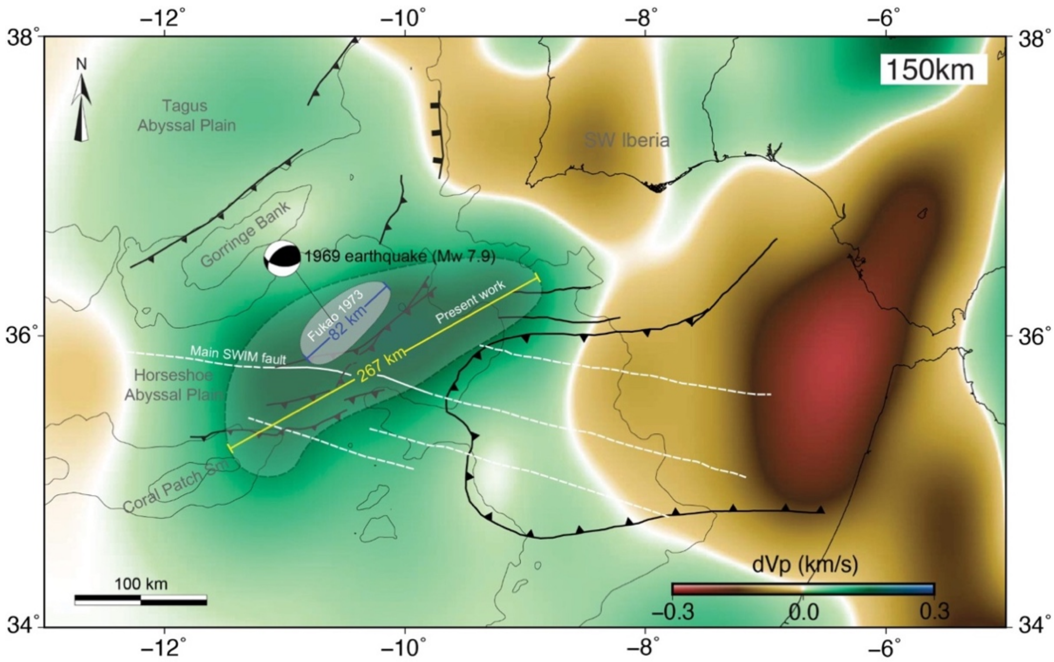

Supplementary Figure 11. Illustration of the rationale behind determining the maximum fault rupture lengths (L) ascribed to the postulated seismogenic structure of the 1969 (M7.9) earthquake. The ~82 km long segment marked in blue corresponds to the fault length implied by the seismogenic domain of the 1969 (M7.9) earthquake as proposed by Fukao[1] based on the distribution of the aftershocks; The ~267 km long segment marked in yellow corresponds to the possible maximum fault length implied by the NW-dipping blind fault discussed in this work and deduced from the projected contour of the high-velocity anomaly.

The relationship between the length of a fault and its magnitude has been empirically established based on differently assumed rheological and seismological parameters for different tectonic settings in different parts of the world[3]. Building on a previous approach[4] a new model has been recently proposed for the study of high magnitude earthquakes in SW Iberia[5]. This model acknowledges different assumptions to infer an average fault slip (d) from the length (L) of the considered seismogenic active fault (Supplementary Fig. 12). This fault-slip is then used together with the fault width (W) and an assumed shear modulus (μ), to obtain the seismic moment (Mo, eq. 1) and the moment magnitude (Mw, eq. 2):

$$M_o = \mu . A . d \qquad \text{(eq. 1)}$$

$$M_w = \frac{2}{3} . log_{10}(M_o) - 6.07 \qquad \text{(eq. 2)}$$

in which A is the rupture area (A = W.L), d is the average slip and μ the shear modulus.

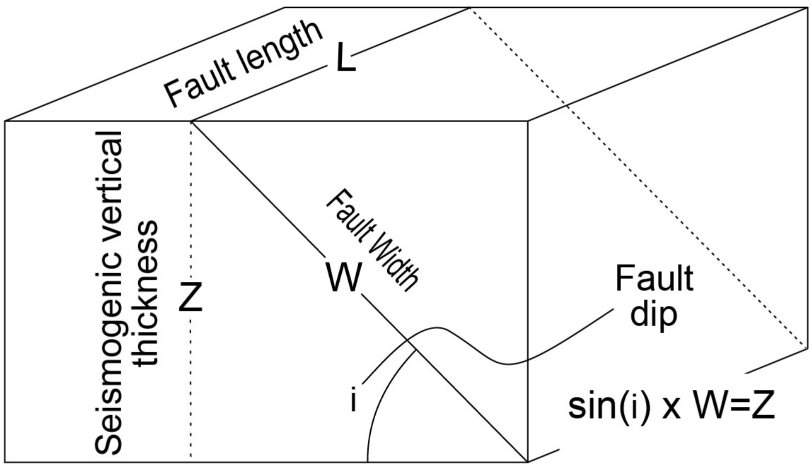

Supplementary Figure 12. Fault Parameters. Geometric fault parameters considered in the discussed seismic scaling laws of Manighetti[4].

The average fault-slip ($d = D_{max}/2$) is calculated as follows:

$$D_{max} \rightarrow \begin{cases} L \leq 2W_{sat} \;\; D_{max} = a\,\frac{L}{2} \\ L > 2W_{sat} \;\; D_{max} = a\,\frac{1}{\frac{1}{L}+\frac{1}{2W_{sat}}} \end{cases} \qquad \text{(eq. 3)}$$

in which a and W_{sat} are the slip/length ratio and the saturation fault width, respectively. These parameters are empirically deduced by the same authors for the study area using the few instrumental high-magnitude events that have occurred in this region. A slightly higher shear modulus of 65 GPa is assumed in this case. Table S1 summarizes the assumptions and input parameters considered to determine the seismogenic potential of the northwards dipping blind-thrust explored in this work (e.g., its rupture area and implied Mo and Mw). Two alternative main fault lengths (L) are considered (Supplementary Fig. S4): one assuming seismic rupture only to the North of the main SWIM Fault; the other considering that the whole structure ruptures during a single event. The first scenario is clearly capable of justifying an event with a magnitude similar to the one of the 1969 (M7.9) earthquake. Likewise, the second whole-rupture scenario is also compatible with the estimated (M8.5-8.7) high magnitude generally ascribed to a 1755-like earthquake.

Supplementary Table 3. Scaling Law of Manighetti[4] modified by Matias[5] used to quantify the seismogenic potential of the postulated blind-fault in the study area.

	Model parameters	**Scenario #1:** rupture to the N of the SWIM fault	**Scenario #2**: whole rupture
Inputs	Fault length L (km)	82	267
	Saturation fault width – Wsat (km)	76	
	Slip-Length ratio (*a* - parameter)	1.8e–4[5]	
	Seismogenic thickness Z (km)	60	
	Fault dip δ (°)	52	
	Shear modulus μ (GPa)	65	
Outputs	Average fault slip d (m)	3.7	8.7
	Rupture area A = W.L (Km2)	5603	20330
	Seismic moment Mo (N.m)	1.34e+21	1.15e+22
	Moment magnitude Mw	**8.0**	**8.6**

References Supplementary Information

1. Fukao, Y. Thrust faulting at a lithospheric plate boundary: The Portugal earthquake of 1969. *Earth Planet, Sci. Lett.* **18**, 205–216 (1973).
2. Purdy, G.M. The eastern end of the Azores–Gibraltar plate boundary. *Geophysical Journal of the Royal Astronomical Society* **43**, 973–1000 (1975).
3. Johnston, A.C. Seismic moment assessment of earthquakes in stable continental regions - III, New Madrid 1811–1812, Charleston 1886, and Lisbon 1755. *Geophys. J. Int.* **126**, 314–344 (1996)
4. Manighetti, I., Campillo, M., Bouleya, S., and Cottona, F. Earthquake scaling, fault segmentation, and structural maturity. *Earth Planet, Sci. Lett.* **253**, 429–438. (2007)
5. Matias, L. M., Cunha, T., Annunziato, A., Baptista, M.A., and Carrilho, F. Tsunamigenic earthquakes in the Gulf of Cadiz: fault model and recurrence. *Nat. Hazards Earth Syst. Sci.* **13**, 1–13. (2013)